ISSN: 3068-2789

Review Article

Journal of All Physics Research and Applications

Observable Strong Interaction in Diamond and Graphene

Plekhanov VG*

Fonoriton Sci. Lab., Garon Ltd., Tallinn 1413, Estonia

***Corresponding author:**
Plekhanov VG, *Fonoriton Sci. Lab., Garon Ltd., Tallinn 1413, Estonia*.

ABSTRACT
Carbon - based materials offer a number of exciting possibilities for both new science and applications. The early measurable change in Eg in the isotope effect of diamond, as in case of LiHxD1_x crystals, is shown a manifestation of the strong interaction that determines the neutron - electron binding energy. Isotopic method provides an alternative way to experimentally tune the band - gap of graphene, which would be more efficient and more contollable than other method that are used to open band - gap in graphene. For the first time, the acquisition of mass in massless Dirac fermions (leptons) from energy of strong nuclear interaction in graphene has been experimentally demonstrated.

Keywords: Strong Interaction, Hadrons, Quarks, Gluons, Excitons, Phonons, QED, QCD.

Received: June 02, 2026;
Accepted: June 10, 2026;
Published: June 17, 2026

PACS

!!@.38 - t; 12.39 - x; 14.20 - o; 78.55 Hx

Carbon, one of the most basic elements in nature, still gives a lot surprises. It is found in many different forms - allotropes - from zero dimensional fullerene, one dimensional carbon nanotubes, two dimensional graphene and graphite, to three dimensional diamond (Figure 1) - and the properties of the various carbon allotropes can vary widely [1].

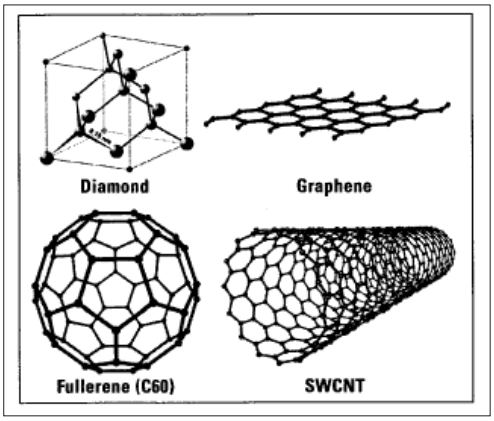

Figure 1: Structure of some representative carbon allotropes

For instance, diamond is the hardest material, while graphite is one of the softest: diamond is transparent to the visible part of spectrum, while graphite is opaque; diamond is an electrical insulator, while graphite is a conductor. Very important is that all these different properties originate from the same carbon atoms, simply with different arrangements of the atomic structure. These carbon materials have attracted particular attention because of their simplicity, different physical size and the exciting new science they have introduced. Carbon atom is built from 6 protons, A neutrons and 6 electrons, where A 6 or 7, yield the stable isotopes ^{12}C and ^{13}C, respectively, and an 8 characterizes the radioactive isotope ^{14}C. The isotope ^{12}C, with nuclear spin I 0, is the most common one in nature with 99% of all carbon atoms, whereas only 1% are ^{13}C with nuclear spin I 1/2. There only traces of ^{14}C (10 12 of all carbon atoms) which - decays into nitrogen ^{14}N. Although ^{14}C only occurs rarely, it is important isotope used for historical dating (see, e.g. [3]). This brief review focuses on each of these materials systems individually (diamond and graphene) and comparatively as example of the appearance new physics.

Citation: Plekhanov VG (2026) Observable Strong Interaction in Diamond and Graphene. J All Phy Res Appli 2: 1-11.

It is well known that isolated carbon atoms have the electronic configuration $1s^2$, $2s^22p^3$ (see, e.g. [2]). However, in the diamond crystal as a result of the formation of the sp^3 hybrid (a mixture of 2s and 2p wave function with tetrahedral bonding) there is a modification of the s - and p - levels which manifests itself in a further splitting of the sp^3 hybrid band into two bands (Figure.), each of which (including spin) can accommodate four electrons. The four electrons of the atomic 2s - and 2p - states thus fill the lower part of the sp^3 band leaving the upper part unoccupied. Between the two sp^3 subbands there is a forbidden energy gap of width E_g.

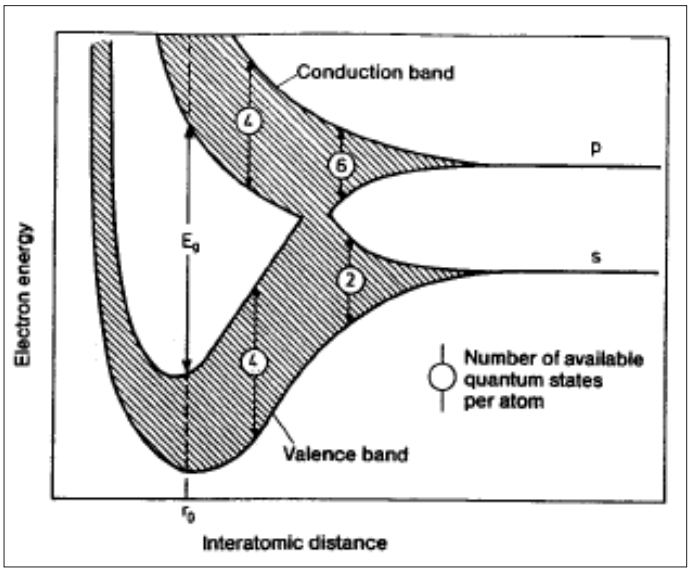

Figure 2: Schematic behavior of the energy bands as a function of atomic separation for the tetrahedrally bound semiconductors diamond (C), Si, and Ge. At the equilibrium separation there is a forbidden energy gap of width E_g between the occupied and unoccupied bands that result from sp^3 hybrid orbitals. For diamond, the sp^3 hybrid stems from 2s and $2p^3$ atomic states.

The four electrons of the atomic 2s and 2p - states thus fill lower part of the sp^3 band, leaving the upper part unoccupied. Between the two sp^3 subbands there is a forbidden energy gap of width E_g. This is the origin of the insulating property of diamond.

In the excitation state, we therefore have four equivalent quantum - mechanical states: 2s, 2px, 2py and 2pz. a quantum - mechanical superposition of the state 2s and n $2p_j$ states is called sp^n hybridization, which play an essential role in carbon bonds [1]. In the case of a superposition of the 2s and two 2p orbitals, which we may choose to be the $2p_x$ and the $2p_y$ states, one obtains the planar sp^2 hybridization. The three quantum - mechanical states are given by

$$|sp_1^2\rangle = \frac{1}{\sqrt{3}}\,|2s\rangle - \sqrt{\frac{2}{3}}\,|2p_y\rangle,$$

$$|sp_2^2\rangle = \frac{1}{\sqrt{3}}\,|2s\rangle + \sqrt{\frac{2}{3}}\left(\frac{\sqrt{3}}{2}\,|2p_x\rangle + \frac{1}{2}\,|2p_y\rangle\right), \qquad (1)$$

$$|sp_3^2\rangle = -\frac{1}{\sqrt{3}}\,|2s\rangle + \sqrt{\frac{2}{3}}\left(-\frac{\sqrt{3}}{2}\,|2p_x\rangle + \frac{1}{2}\,|2p_y\rangle\right).$$

These orbitals are oriented in the xy - plane and have mutual 120^0 angles (Figure. 3[a]). The remaining unhybrized $2p_z$ orbitals perpendicular to the plane A prominent chemical example for such hybridization is the benzene molecule [2]. This molecule consists of a hexagon with carbon atoms at the corner linked by bonds (Figure 3[b]). Each carbon atom has, furthermore, a covalent bond with one of the hydrogen atoms which stick out from the hexagon in a star like manner. In addition to the 6 bonds, the remaining $2p_z$ orbitals form 3π bonds, and the resulting double bonds alternate

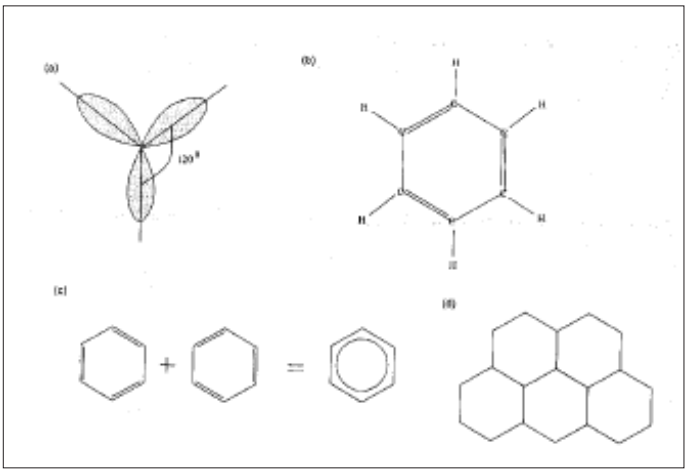

Figure 3: (a) Schematic view of the sp^2 hybridization. The orbitals form angles of 120^0. (b) Benzene molecule - C_6H_6. The 6 carbon atoms are situated at the corners of a hexagon and form covalent bonds with the H atoms. In addition to the 6 covalent σ bonds between C atoms, there are three π bonds indicated by the doubled line. (c) The quantum - mechanical ground state of the benzene ring is a superposition of the two configurations which differ by the position of the π bonds. The π electrons are, thus, delocalized over the ring. (d) Graphene may be viewed as a tiling of benzene hexagons, where the H atoms are replaced by C atoms of neighboring hexagons and where the π electrons are delocalized over the whole structure.

with single σ bonds around hexagon. Because a double bond is stronger than a single σ bond, one may expect that the hexagon is not perfect. A double bond (C = C) yields a carbon - carbon distance of 0.135 nm, whereas it is 0.147 nm for a single σ bond (C - C). However, the measured carbon - carbon distance in benzene is 0.142 nm for all bonds, which is roughly the average length of a single and a double bond. The ground state a quantum - mechanical superposition of the two possible configurations for the double bonds shown schematically in Figure 8[c]. These chemical considerations indicate the way towards carbon - based condensed matter physics any graphitic compound has been a sheet of graphene as its basic constituent. Such a graphene sheet may be viewed simply as a tiling of benzene hexagons, where one has replaced the hydrogen by carbon atoms to form a neighboring carbon hexagon (see Figure 3[d]). However, graphene has remained the basic constituent of graphitic systems during a long time only on the theoretical level. From experimental point of view, graphene is the youngest allotrope and accessible to physics measurements only since 2004. Graphite may be viewed as a stacking sheet (Figure.8[e]) that stick together due to the

van der Waals interaction, which is much weaker than in plane covalent bonds.

If one superimposes the 2s and all three 2p orbitals, one obtains the sp^3 hybridization, which consist of four club - like orbitals that mark a tetrahedron. The orbitals forma angles of 109.5^0 degrees (Figure 4[a]). A chemical example for this hybridization is methane (CH_4), where the four hybridized orbitals are used to form covalent bonds with the 1s hydrogen atoms. In condensed matter physics, the $2p^3$ hybridization is at the origin of the formation of diamonds, when liquid carbon condenses under high pressure. The diamond lattice consists of two interpenetrating face - center - cubic (fcc) lattice as, with a lattice spacing of 0.357 nm as shown in Figure 4[b].

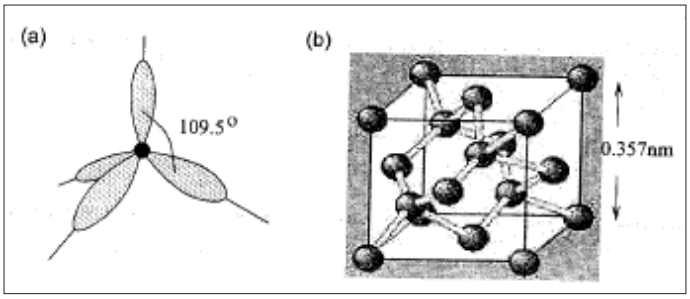

Figure 4: (a) sp^3 hybridization with 109.5^0 angle between the four orbitals. (b) Crystal structure of diamond.

Diamond has, perhaps, he simplest and most basic covalent band structure. Figure 5 shows the electronic energy - band along several lines of high symmetry from the center (Γ) to boundary of the first Brillouin zone (BZ) as calculated LCAO method in paper [4].

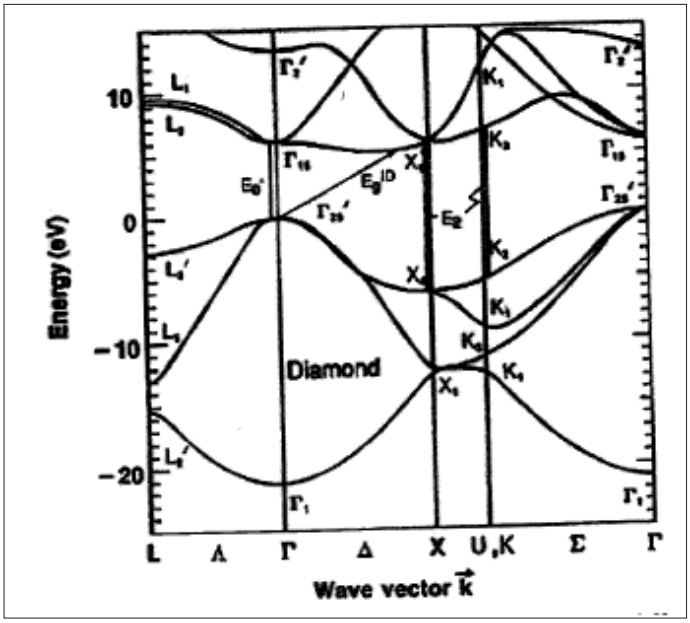

Figure 5: Electronic band - structure of diamond along several lines of high symmetry to the boundary of the first BZ as calculated with a modified LCAO method [4].

The electronic states are labeled using the notation for the single group of the diamond structure. The location of several interband transitions is included by the vertical arrows. The fundamental absorption edge of diamond corresponds to indirect transitions from highest valence band at the point to the lowest conduction band in the Δ direction (X point) (i.e. $\Gamma_{25} \rightarrow \Delta 1[X_1]$) (see also [5,6]). Like Si (see, e.g. [7]) the lowest - lying conduction band at point of BZ in diamond, Γ_{15} is p - like, however, as we can see, in Ge the s - like Γ_2 band is the lowest conduction band [7]. As mentioned in literature one common characteristic of all published spectra in the ultraviolet region of diamond is the presence of two major peaks at -7.02 - 7.4 and -12.2 - 12.7 eV [7]. The first peak may originate from transition (E'_0) and the second one from $X_4 \rightarrow X_1$ and $\sum_2 \rightarrow \sum_1$ transition (E_2) (the more detail see [6]).

Due to the indirect gap of E_g=5.47±0.005eV (295K), at K=0.76X, diamond has intrinsic phonon - assisted free exciton luminescence lines (see, e.g. [8]). The change of the indirect gap of diamond between pure ^{12}C and ^{13}C crystals has been determined by Collins et al. [9]. The luminescence spectra of the natural (^{12}C) and synthetic (^{13}C) diamond at electron excitation were investigated by Collins et al. (Figure. 10), Ruf et al., Watanabe et al. [9-11]. Figure. 6 compares the free exciton luminescence for a natural diamond with that for a synthetic diamond.

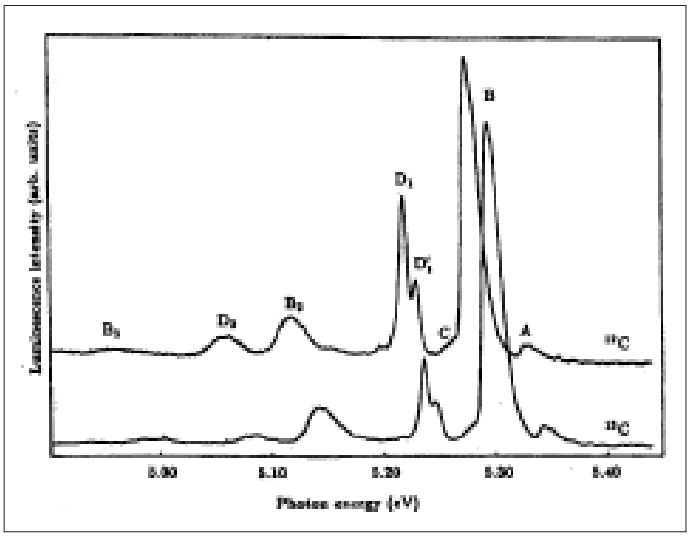

Figure 6: Spectra measured at 77K phonon - assisted free cathodoluminescence feature (A, B and C) and the phonon assisted bound - exciton feature (D) from natural semiconducting ^{12}C diamond and a ^{13}C synthetic diamond (after [9]).

The peaks labeled A, B and C are due, respectively, to the recombination of a free exciton with the emission of transverse - acoustic, transverse - optic and longitudinal optic phonons having wavevector $\pm k_{min}$ and quanta in ^{12}C [8, 12].

$$h\omega_{TA} = 87 \pm 2;\ h\omega_{TO} = 141 \pm 2;\ h\omega_{LO} = 163 \pm 1 \text{ meV}. \quad (2)$$

Features B2 and B3 are further free exciton processes involving the above TO phonon with one and two zone - center optic phonons respectively. As we can see from Figure. 12 the isotope shift of the free exciton luminescence spectrum of ^{13}C diamond is equal 16.5 ± 2.5 meV [8, 12]. The more detailed and quantitative investigation of $E_g \sim f(x)$, where x is the isotope concentration

was done by Ruf et all. (Figure. 7) and Watanabe et all. (Figure. 8) where five samples of diamond with different concentrations x were studied [10,11].

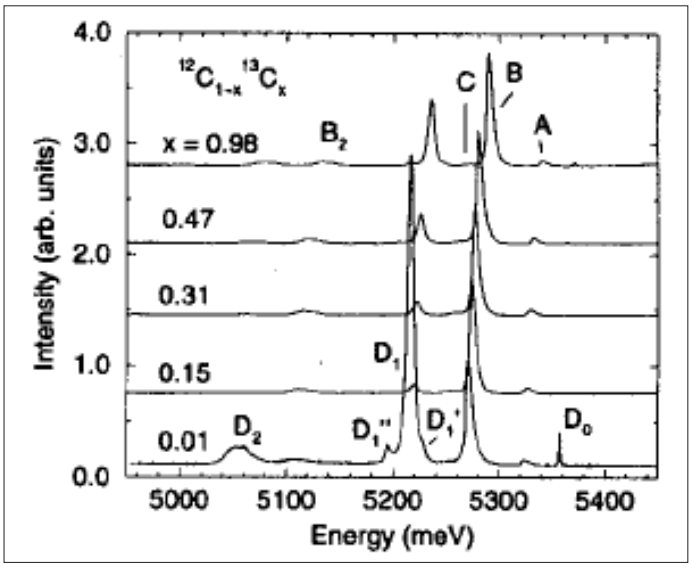

Figure 7: Cathodoluminescence spectra of isotopically modified diamond at 36 K. Intrinsic phonon - assisted recombination peaks are labeled in the top spectrum, those from boron - bound excitons in that at the bottom. The spectra are normalized to the intensity of the B peak and vertically offset for clarity (after [10]).

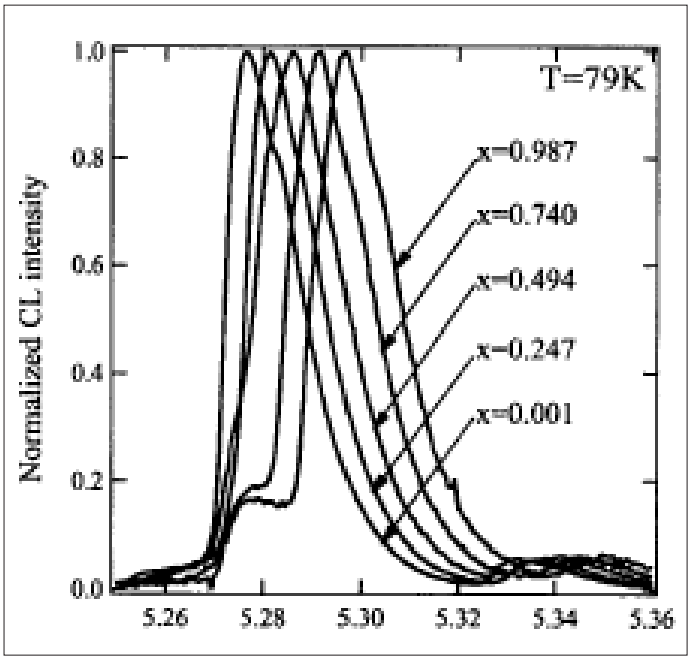

Figure 8: luminescence spectra of free excitons in homoepitaxial diamond films grown from mixture of methane in hydrogen by means of a microwave plasma assisted CVD. The spectra illustrate the effect of isotope composition $^{12}C^{13}1_xC_x$ mixed in the CVD gas phase. All spectra ate normalized to the same height (after [11]).

Watanabe et al. have concluded that the maximum change of the band gap due to substitution of ^{12}C by ^{13}C is ΔE_g 15.4 meV. This value (15.4 meV) is in good agreement with the estimate of 16.5 ± 2.5 meV by Collins et all. [9] using a zero-point renormalization obtained from a fit of the experimental temperature dependence of the band gap. We should stress that the isotope shift in $^{12}C^{13}{}_xC_{1-x}$ diamond crystals approximately 15 meV per one neutron and on seven neutrons we get 15 - 7 = 105 mev. This value is very close to the observed one (103 meV) in $L_iH_xD_{1-x}$ crystals - value of neutron - electron binding energy [13]. As will be shown below this value is the maximum value of the neutron - electron binding energy.

It is clear that the lattice - dynamic properties of a crystal are directly affected by the atomic mass. To a first approximation, phonon behave like harmonic oscillators with frequencies [14]

$$\omega \alpha m^{-1/2}. \quad (3)$$

Crystals containing various isotopes are usually described within virtual crystal approximation (VCA) [8] where m in Eq. (3) is replaced by the average atomic mass

$$\bar{m} = \sum_i c_i m_i. \quad (4)$$

It is obtained from the sum over the isotope's masses m_i and concentration c_i. In spite of VCA simplicity, the model describes the general feature of the lattice dynamics of mixed alkali - halide crystal sufficiently well (for details see [14, 15]). Isotopes are ideal for lattice - dynamitic investigations of crystals. One can make use of the unique isotopic properties by varying the isotopic composition. Isotope substitution helps to disentangle the individual contributions of anharmonic and disorder - induced effects and to clarity the origin of phonon broadening mechanisms. Due to the fact that substitution of the isotopic mass in semiconducting crystals a small variation of E_g, perturbation theory is applicable (excluding LiH crystals [8,12]).

Raman spectroscopy is a powerful means to gain experimental access to phonons and their interaction and scattering mechanisms. All studies presented in this paragraph are restricted to stable, i.e. non - radioactive isotopes. About 300 stable and 1000 radioactive isotopes are known today. Some elements are isotopically pure (for example, Co), while others may contain numerous isotopic modifications (for example, Sn has 10 stable isotopes with atomic masses ranging from 112 to 124, while Xe has 23 isotopes, 9 of which are stable (see, Table 1 in [12]).

It is well - known that materials having a diamond structure (C, Si Ge, - α - Sn) are characterized by the triply degenerate phonon states in the Γ - point of the Brillouin zone $(\vec{k} = 0)$ (see, e.g. [15]). Isotope effect in light scattering spectra in Ge crystals was first investigated by Agekyan et al. [16]. A more detailed study of Raman light scattering spectra in isotopically mixed Ge crystals has been performed by Cardona and coworkers [12].

The cubic modifications of crystalline carbon, diamond, is characterized by a tetrahedral coordination underlying its structure dictated by sp^3 bonding (see Figure. 4) between the nearest neighbor atoms. Diamond has two atoms per primitive (Bravais) cell. The strong covalent bonding and the light mass of the constituent atoms result in a large frequency for zone center, Raman active, triply degenerate F_2 mode [15]. Its crystalline

perfection and transparency make diamond ideally suited for inelastic light scattering [2]. First Raman study of the dependence the frequencies of phonons on the isotopic composition was conducted on diamond by Chrenko in 1988 [17]. Most clear results was obtained by Hanzawa et al. [18] (see Figure. 14).

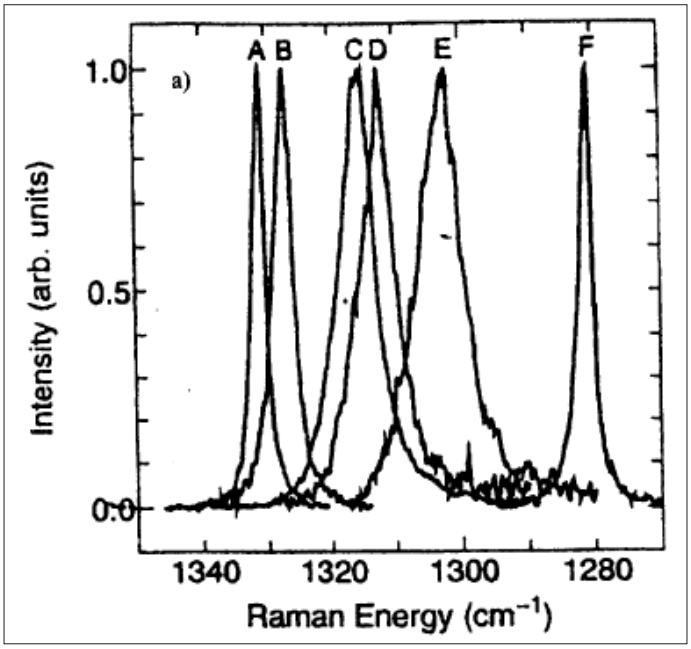

Figure 9: First - order Raman scattering in isotopically mixed diamond crystals $^{12}C^{13}_{x}C_{1-x}$. The peaks A, B, C, D, E and F correspond to x 0.989; 0.90; 0.60;
0.50; 0.30 and 0.001(after [18]).

First - order Raman light scattering spectrum in diamond crystals also includes one line with maximum $\omega_{LTO}(\Gamma) = 1332.5$ cm^{-1} [18]. In Figure. 9 the first - order scattering spectrum in diamond crystals with different isotope concentrations is shown. As was shown in, the maximum and width of the first - order scattering line in isotopically - mixed diamond crystals are nonlinearly dependent on the concentration of isotopes x [12]. The maximum shift of this line is 52.3 cm^{-1}, corresponding to the two limiting values of x 0 and x 1. The effect of the isotopic ^{12}C to ^{13}C ratio on the first - and second - order Raman scattering of light in the diamond has been investigated in [19]. As ^{13}C content is increased from the natural ratio ($^{12}C/^{13}C$ (1-x)/x, where x 0.011 to the almost pure ^{13}C (x = 0.987) the whole spectrum has shifted towards longer wavelength (Figure. 10) in good agreement with the expected $M^{-0.5}$ frequency dependence on the reduced mass M. For an approximately equal mix of the two isotopes, the authors reported that the feature seen in the above two phonon spectra were either broadened or unresolved.

The measured dependence on average mass mainly reflects the isotope effect on the harmonic frequency (Eq. (3)) which is, however, modified by anharmonic and disorder - induced contributions [8, 12]. Isotope renormalization frequencies of phonons of other semiconducting crystals (GaP, GaAs, - α - Sn, ZnS, ZnO, CuCl, CuBr) was published in the next reviews [12, 20]. We should highlight that addition one next neutron in nuclei is called the change in more or less of energy of elementary excitations in solids.

The science of the nuclear, atoms, simple molecules and the science of matter from microstructure to larger scales are well established. A remaining, extremely important, size related challenge is at the atomic scale, roughly the dimensional scale between 1 and 10 molecular sizes, where the fundamental properties of materials are determined and can be engineered (see also [8,12,23]. This field of science - isotopetronics - is a broad and interdisciplinary field of emerging research and development. Isotopetronics is connected to materials, structures and systems which components, as in nanoscience, exhibit novel and significantly modified physical properties due to their small sizes [21]. The method of the isotope renormalization of the energy of elementary excitations in bulk solid and low - dimensional structures very often used in the last five decades and well documented in the scientific literature (see [8,12] and references quoted therein).

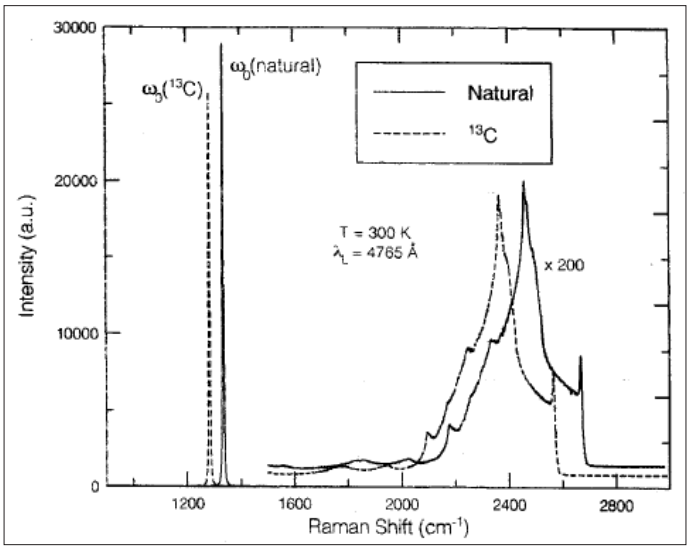

Figure 10: The Raman spectra of natural and a ^{13}C diamond. The spectra show the dominant first - order Raman - active F_{2g} line and the significantly weaker quasi - continuous multiphonon features (after [19]).

The discovery of global changes in macroscopic, including optics, properties upon the addition of one neutron made the unique crystals of LiH and LiD (diamond, graphene), which differ by one neutron, an excellent model for studying the strong interaction [22]. We have previously emphasized the importance of using low temperature spectroscopy to study strong nuclear interaction [23]. Let us add in this regard that a recently published sensible, informative review the author adheres to the already traditional direction of searching for new physics and the origin of mass beyond the SM boundary in high - energy physics by more powerful accelerators [24]. It is worth recalling that already in work the clarification of the origin of the observed world was linked with the nucleon mass [25]. To clarify this, it is necessary to understand the mechanism of breaking chiral symmetry (symmetry of the equations of motion due to the asymmetry of the Universe in QCD (for more details, see [26] and the literature cited there). This author has shown that the breaking symmetry occurs at large distances of $\simeq 1$ fermi = 10^{-15}m, and thus has no relation to high - energy experiments investigating small distances of 10^{-19} m (see more details [25, 26]). Incidentally, we

note that after our work on strong interaction in the mass isotope effect, a whole of works appeared devoted to the search for new physics in the isotope effect of heavy chemical elements [26-32]. In other words, following us in those works, they are also trying to find a new type of boson interacting with a neutron and an electron.

It is well known from atomic spectroscopy that the isotopic shift of spectral lines arises as a result as a result of the shift relative to each other of the energy levels of atoms belonging to different isotopes of the same chemical elements [33]. This displacement is a result of the interaction of the electron shell with the nucleus. Therefore, the isotopic effect should manifest both the properties of the nucleus and the characteristic features of the electron shell. As noted earlier, the phenomenologically mass isotopic shift is caused by the correction of the kinetic energy of the atomic electrons by the motion of the nucleus and is described by formula

$$E = \frac{1}{2}\left(\frac{1}{m_e} + \frac{1}{M}\right)\sum_i p_i^2 + \frac{1}{M}\sum_{i=j} p_i p_j. \quad (5)$$

Here m_e and M are the mass of the electron and the nucleus, p_i and p_j are the momenta of the i - th and j - th electrons. It is the first term of last relation that describes the isotopic shift in light elements. The second term describes the specific mass isotope shift and is due to the electron's interaction. Quantum - mechanically, this interaction is described by the electron - phonon model [34]. The quantum mechanical solution to the task of electron - phonon interaction (in our case, neutron - electron interaction) is found taking into account the adiabatic approximation, which takes into account that mass of an electron is approximately 2000 times less than the mass of a nucleus [35]. The latter allows the use of perturbation theory.

The use of the adiabatic approximation leads to the appearance of non - adiabatic term, which is neglected due to its smallness (see formula 5 in [34,36]). It is precisely the neglect of the non - adiabatic term that allows us to reduce the given problem to two independent Schrödiger equations - electronic and nuclear. As shown in work, the electron equation does not depend on the mass of the nucleus, and therefore the energy eigenvalue are the same for different isotopes [36]. This conclusion, as well as the large of the isotopic shift energy, makes it necessary to search for new mechanism to describe the neutron - electron interaction, including subatomic physics [23]. As easy shown early, in the case of LiD and LiH crystals the difference between zero phonon emission lines in the low - temperature luminescence specters is equal to the neutron - electron binding energy equal 0.103 eV [23,37]. Similarly, in the case of diamond crystals of different isotopes such difference determines the neutron electron binding energy equal 0. 105 ± .002 eV. It was shown early that neutron electron binding energy in Ge and ZnO it is equal to 108 ± 5 and 122 ± 10 meV, respectively. Data for Ge and ZnO crystals are taken from review [37]. A good agreement is evident with the data of Breit (106.7 meV) obtained from the results of scattering of electrons (their length) more than half a century ago in the electrostatic model [38,39]. Naturally with an increase in the number of nucleons in the nucleus, it is necessary to take into account the field contribution, which was not done in our estimates [33]. Thus, spectroscopic measurements of the mass isotopic shift it possible for the first time to determine the neutron - electron binding energy. Using subatomic physics to interpret the results of measuring the strong interaction from the distance between the proton and neutron in the deuterium nucleus in LiD crystals allows us to estimate the energy of the boson responsible for the interaction of the neutron and electron and secondly to calculate the coupling constant of the strong interaction at different values of the binding energy. For an interaction radius equals to the Bohr radius a_0 0.52917706 . 10^{-10} m, the Yukawa potential gives a boson mass value of ≃ 3.7 keV* [40].

Relativistic units ($= c = 1)\hbar$ were used to obtain this estimate.

Another carbon - based material is the recent discovery of graphene, a single atomic monolayer of carbon, has opened up a new field of fundamental physics and offers exciting prospects for new electronic devices (see, for example review [14]). Graphene consists of a single sheet of carbon atoms bonded in the sp^2 configurational of a hexagonal structure (Figure. 1). Such an atomic structure is characterized by two types C - C bonds (σ, π) constructed from four valence orbitals (2s, $2p_x 2p_y$, $2p_z$), where z directionis perpendicular to the sheet. Three σ - bonds join a C atom to its three neighbors. In addition, the C - C bonding is enhanced by a fourth bond associated with the overlap of p_z (or π) orbitals. A two - dimensional sp^2 graphene containing two atoms per unit cell, A and B (Figure. 11[a]). When two graphene sheets are stacked, what is called bilayer graphene is obtained (Figure. 11[b]).

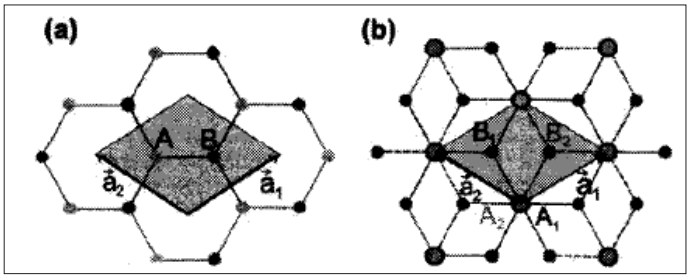

Figure 11: Schematics showing the structure of sp^2 graphene. .a-monolayer graphene, the two vectors $\vec{a_1}$ and $\vec{a_2}$ define the unit cell (gray rhombus) containing two atoms A and B. b - bilayer graphene, the unit vector, unit cell, and the four atoms (A_1, B_1 from one layer plus A_2, B_2 from the other) within the unit cell are displayed.

Graphene, because of its structural simplicity (two atoms per unit cell), has been extensively investigated in theory for the past some decades [41 - 43]. Theoretical calculations show that the π - band overlap in graphite disappears as the layers are further separated over their equilibrium distance in graphite. This leads to decoupled graphene layers that can be described as a zero - gap semiconductor. The π - band electronic dispersion for graphene near the six corners (see, for example Figure. 6 in chapt. 5 in reference) of the 2D hexagonal Brillouin zone is found to be linear [23]. The linear electronic band dispersion leads to the term "massless Dirac fermions" for these carriers [14]. Figure

12 shows the ab - initio calculations of the electronic band of graphene along the high - symmetry M - Γ - K directions [43].

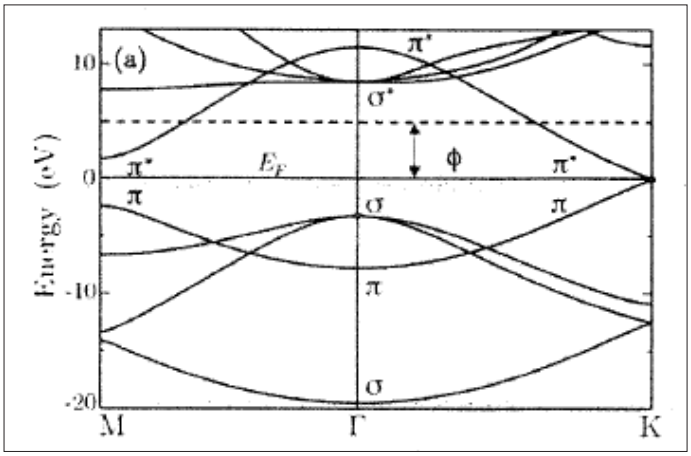

Figure 12: Electronic band structure of graphene from ab intio calculations [43]. The bonding σ and antibonding σ^* bands are separated by a large energy gap. The bonding π (highest valence band) and the antibonding π^* (lowest conduction band) bands touch at the KK' points of the Brillouin zone.

Figure 13 shows the graphene honeycovb lattice consists of two triangular sublattices as well as the first Brillouin zone along the highest symmetry M - Γ - K directions.

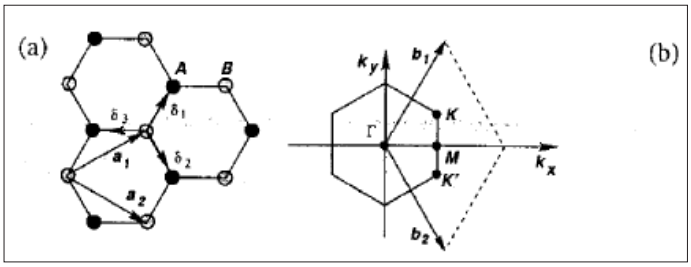

Figure 13: a - graphene honeycomb showing the two triangular sublattices, b the graphene Brillouin zone in momentum space.

As it can be seen from Figure. 6 - 9 the band gap of ^{13}C has increased by 13.6 meV. Numerous examples of band gap increasment at hard isotope substitution were collected in the papers [8, 12]. The effect of the isotopic ^{12}C to ^{13}C ratio on the first and second - order Raman scattering of light in the diamond has been investigated in [17, 14]. As the ^{13}C content is increased from the natural ratio (^{12}C/ ^{13}C (1 - x) / x, where x 0.011), to the almost pure ^{13}C (x 0.987), the whole spectrum has shifted towards longer wavelengths (see Figure. 6) in good agreement with the expected $M^{-0.5}$ frequency dependence on the reduced mass M. For an approximately equal mix of the two isotopes, the authors reported that the features seen in the above two - phonon spectra were either broadened or unreasonable. We should stress that the main line in the first - order Raman scattering spectrum of light at ω 1332 cm^{-1} also shifts to the short-wavelength side on the 52.3cm^{-1} [8,12].

Raman spectroscopy for the various sp2 carbon materials (see Figure 14) has been mainly used for simple characterization and these different carbon materiald exhibit characteristic differences related to the small differences in their structure. As was shown above the fundamental sp^2 carbon material is mono - layer graphene which has the simplest and most fundamental spectrum showing the two Raman - allowed features that appear in all sp^2 carbon materials - the first - order G - band (around 1580) and the second - order symmetry - allowed G' - band (around 1360 cm^{-1}), where the symbol G is used to denote "graphitic". The next most commonly observed feature is the D - band that is defect - activated Raman mode [14]. Elastic and inelastic light scattering are powerful tools for investigating graphene [76-81]. Raman spectra of graphene and graphite measured at room temperature and at the excitation at E_{laser} 2.41 eV (514.5 nm) is depicted on Figure. 14.

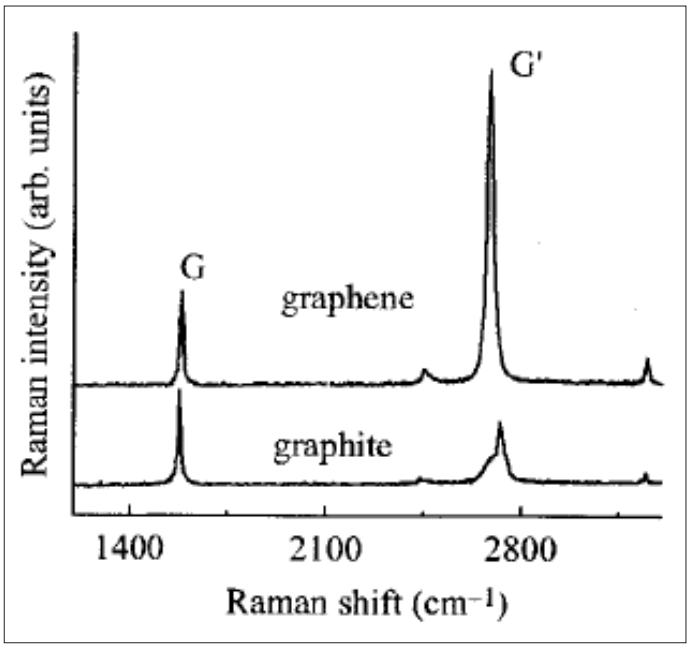

Figure 14: Comparison of the Raman spectra of graphene and graphite measured at room temperature and at the excitation at E_{lase} = 2.41 eV (514.5 nm).

The G peak (see, also Figure. 14) corresponds to the E_{2g} phonon at the Brillouin zone center (Γ- point). The D peak is due to the breathing modes of six - atom rings and requires a defect for its activation. It comes from TO phonons around the Brillouin zone K point and it is activated by an intravalley scattering process. The 2D peak is the second order of the D peak. This is a single peak in monolayer graphene, whereas it splits into four bands in bilayer graphene, reflecting the evolution of the band structure [14,23]. The Raman spectrum of graphene also shows significantly less intensive defect - activated peaks such as the D' peak, which lies at ~ 1620 cm^{-1}. This is activated by an intravalley process i.e. connecting two points belonging to the same cone around K (see, Figure. 6 in [23]). The second order of the D' peak is called 2D' peak. Since 2D and 2D' peaks originate from a Raman scattering process where momentum conservation is obtained by the participation of two phonons with opposite wave vector ($\vec{q}$ and $-\vec{q}$), they do not require the presence of defects. Thus, they are always visible in the Raman spectrum (see cited papers [14, 23] and references therein).

Graphene is one unique material which shows properties not fond in other materials. One of these unique features of graphene

is the influence of long-range strains on the electronic properties. The possibility of tuning the dynamics of carriers as well as phonons by appropriately designed strain patterns opens the way for novel applications of graphene, not possible with any other materials. At present time we have several reports, which have examined graphene properties under uniaxial deformation [14, 23, 44-46].

Strain can be very efficiently studied by Raman spectroscopy since this modifies the crystal phonon frequency, depending on the anharmonicity of the interatomic potentials of the atoms. Raman spectra of strained graphene show significant redshifts of 2D and G band (see Table 1) because of the elongated of the carbon - carbon bonds.

Table 1. Red shift of the G and 2D bands in the Raman spectra in graphene monolayers under uniaxial tensile stress.

Ref.	Shift of G (G^+ and G^-) band cm^{-1}/%	Shift of 2D band cm^{-1}/%	E_g, meV
23	14.2	27.8	300
44	5.6; 12.5	21	
45	10.8; 31.7	64	
50 theory			$\simeq$ 500

In order to make graphene a real technology, a special issue must be solved creating an energy band - gap in the Brilloin zone (see Figure. 15). Different attempts have been made by researches, such as patterning graphene into nanoribbon, forming graphene quantum dots, making use of multilayer graphene sheets and applying an external electric field [47-49]. It was shown that the uniaxial strain can open a band gap in a metallic carbon nanotube as well as carbon nanoribbon.

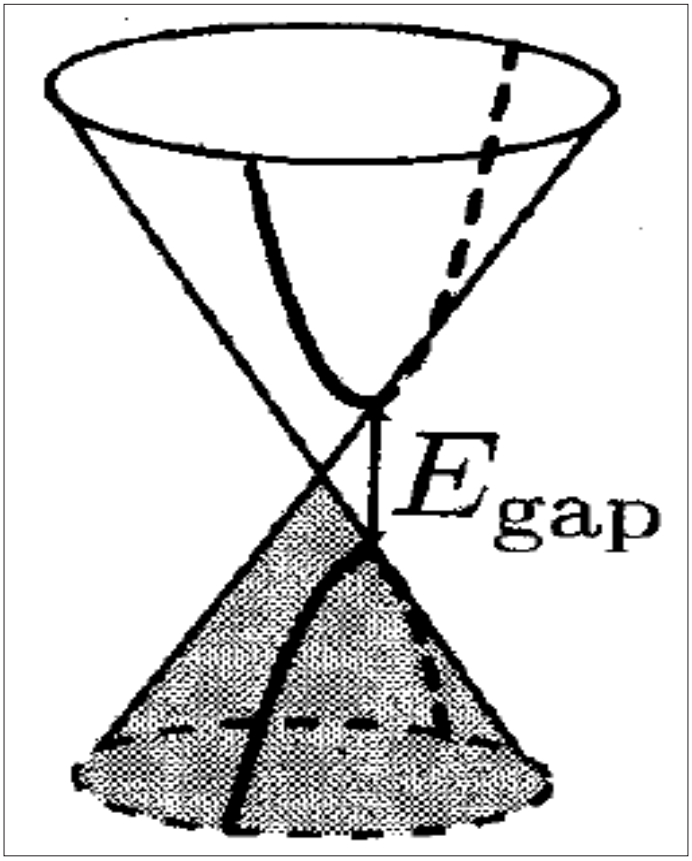

Figure 15: The energy dispersion of semimetal (solid line) and semiconder (dashed line) graphene.

The authors of the paper have proposed that by applying uniaxial strain on graphene, tunable band - gap at K - point can be realized [45]. First principal calculations predicted a band - gap opening of $\simeq$ 300 meV for graphene under 1% uniaxial tensile strain (Figure. 16). Thus, the strained graphene provides an alternative way to experimentally tune the band - gap of graphene, which would be more efficient and more contollable than other methods (see, above) that are used to open band - gap in graphene.

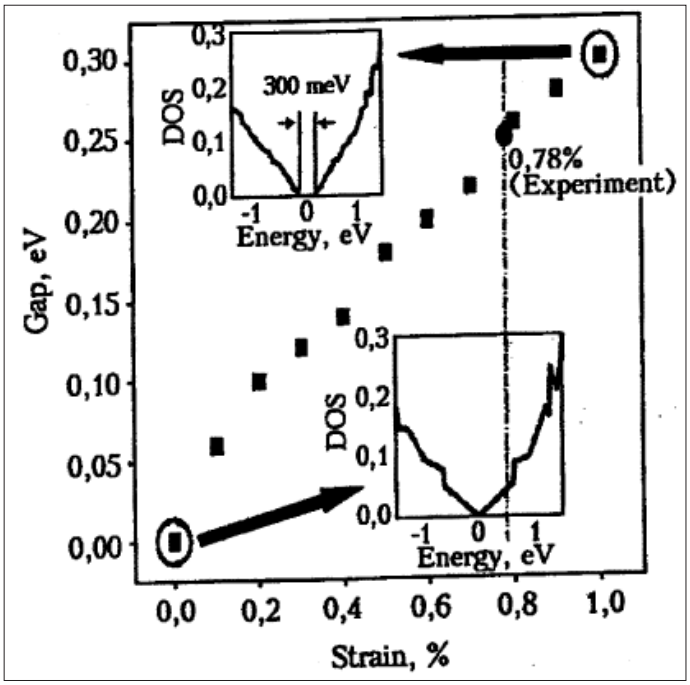

Figure 16: The band - gap of strained graphene with the increase of uniaxial tensile strain on graphene. The magnitude of gap is determined by the gap opening of density of states. The insets show the calculated density of states of unstrained and 1% tensile strained graphene. The dash line and solid dot indicate the calculated bandgap of graphene under the highest strain (0.78 %) [45].

The method of the isotope renormalization of the energy of elementary excitations in solid very often used in last five decades and well described in the scientific literature (see, for example reviews [8,12,20]). At now there is a large list of the paper devoted to investigation of the isotope - mixed graphene [14,23,50]. Chen at al. have reported the first experimental study of the isotope effect on the thermal properties of graphene [51]. The thermal conductivity K, of isotopically pure ^{12}C (0.01 of ^{13}C) graphene determined was higher than 4000 W/mK (approximately two times more than it in diamond) at the measured temperature $T_m \sim 320K$, and more than a factor of two higher than the value of K in a graphene sheets composed of a 50% - 50% mixture of ^{12}C and ^{13}C [23,12]. Raman spectroscopy transferred to the 285 nm SiO2/Si wafer was performed under 532 nm laser excitation (Figure. 16) [51]. The G peak and 2D band positions in Raman spectra of graphene with 0.01%, 1.1%, 50% and 99.2% ^{13}C - isotope are presented in Figure. 17.

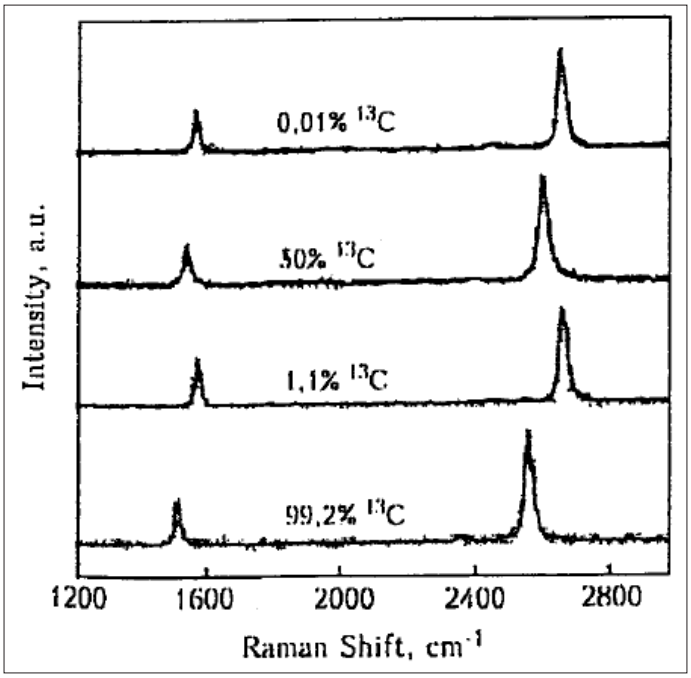

Figure 17: Raman spectra of graphene with different isotope concentration at room temperature [51].

Isotope shift of the G and 2D bands in the Raman spectra depicted on the Figure.18 [52].

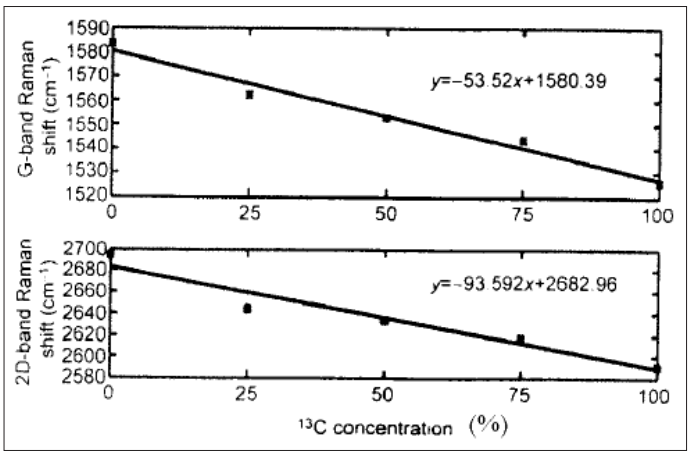

Figure 18: Peak position of G and 2D bands in Raman spectra as a function of the concentration of ^{13}C [52].

As in the case of isotope - mixed diamond the Brillouin - zone - center optical - phonon frequency varies with the atomic mass M as $\omega \sim M^{-1/2}$ making the Raman shift for ^{13}C approximately $(12/13)^{-1/2}$ times smaller than that for ^{12}C [8, 12, 9]. The experimental difference between the lowest 99.2% ^{13}C and the highest 0.01% ^{13}C peak is ~ 64 cm^{-1} which is according in agreement with the theory, and attests for the high quality of isotopically modified graphene [9]. By the way we should indicate that in the Raman spectra in diamond (with sp^3 - bond) analogous shift of first - order line in Raman spectrum is equal 52.3 cm^{-1}, which is consistent with the isotope mass ratio [19]. Substituting a light isotope (^{12}C, H) with a heavy one increases the interband transition energy in the case $^{12}C^{13}{}_xC_{1-x}$ on 14.7 meV and LiH_xD_{1-x} on 103 meV [23].

Graphene has a two lattice parameters *d* and *a* [44]. When replacing the light ^{12}C isotope with the heavy ^{13}C isotope, a change in the parameters of the graphene hexagon is observed. The lattice constant d = 2.46Å increases by 5%, while the magnitude an increase from 1.42Å to 1.5441 Å [44,53]. As it can easily see $\Delta a/a$ 8%. Since a hexagon of graphene transforms into rectangual (Figure. 18) when stress is applied the average change in tension (compression) of graphene is average of 6.5% at the isotopic effect [50].

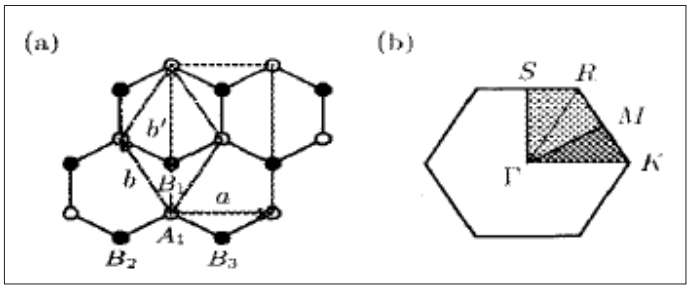

Figure 19: a) Graphene honeycomb lattice. It is formed from a triangular Bravais lattice with a two - atom basis consisting of A_1 and B_1, under uniaxial strain the Bravais lattice becomes centered rectangular. b) First Brillouin zone [50].

Using the results of the work of the authors we come to the conclusion that the isotopic effect causes an opening band gap in graphene up to a value equal to 1.95 eV [23, 45]. Thus, the introduction of an additional neutron into the carbon nucleus (^{13}C) increases the strong interaction according Yukawa the influence of which on the electron (lepton) in graphene stimulates the opening of the band gap [40]. The resulting E_g in ^{13}C graphene is quite close to value E_g 3.4 – 3.7 eV hydrocarbon as well as fluographene [54,55].

With the opening E_g of massless fermions (leptons = electrons) acquire mass. estimates of different ways of opening E_g in graphene give the following equality: E_g 2m, [56]. When E_g 1.95 eV leptons acquire a mass equal 0.975 eV - the value is not large, but finite. One of the mechanisms of acquire mass in elementary particle physics is considered early [57]. This paper predicts that both quarks and gluons acquire running mass distribution in

QCD, which are large at infrared momenta. Roberts shows that gluons are cannibals: they are particle species whose members become massive by eating each other [58].

Conclusion

The artificial activation of the strong nuclear activation by adding one (two, etc) neutron to an atomic nucleus leads to direct observation of the macroscopic properties of the long - range strong nuclear interaction [59]. Our non - accelerator experiments allowed us to measure for the first time the neutron - electron binding energy equal 106 meV, which is in good agreement with the theoretical estimate of 106.7 meV. Isotopic method provides an alternative way to experimentally tune the band - gap of graphene, which would be more efficient and more contollable than other method that are used to open band - gap in graphene [60]. For the first time, the acquisition of mass in massless Dirac fermions (leptons) from energy of strong nuclear interaction in graphene has been experimentally demonstrated. The uniqueness of the isotope effect in the study of elementary particles dynamics in nuclear physics is emphasized.

References

1. Field JE (1992) The properties of Natural and Synthetic Diamond. Academic Press, New York.
2. Harrison WA (1980) Electronic Structure and Properties of Solids. S.W.Freeman and Co., San Francisco.
3. Plekhanov VG (2012) Isotopes in Condensed Matter. Springer, Heidelberg.
4. Chelikowsky JR, Louie SG (2013) First principles linear combination of atomic orbitals method for the cohesive and structural properties of solids: Application to diamond. Phys. Rev. B 29: 3470-3482.
5. Clark CD, Dean PJ, Harris PV (1964) Intrinsic edge absorption in diamond. Proc. Roy. Soc. (London) A 277: 312-329.
6. Vavilov VC, Gippius AA, Konorova EA (1985) Electron and Optical Processes in Diamond. Science, Moscow. (in Russian).
7. Yu PY, Cardona M (1996) Fundamentals of Semiconductors. Springer, Berlin.
8. Plekhanov VG (2005) Elementary excitations in isotope - mixed crystals. Phys.Repors 410: 1-235.
9. Collins AT, Lawson SC, Kanda K (1990) Indirect energy gap of 13C. Phys. Rev. Lett 65: 891-893.
10. Ruf T, Cardona M, Pavone P (1998) Cathodoluminescence investigation of isotope effect in diamond. Solid State Commun 105: 311-316.
11. Watanabe H, Koretsune T, Nakashina S (2013) Isotope composition dependence of the band - gap energy in diamond. Phys. Rev. B 88: 205420-205425.
12. Cardona M, Thewalt MLW (2005) Isotope effects on the optical spectra of semiconductors. Rev. Mod. Phys 77: 1173-1224.
13. Plekhanov VG (2018) Phenomenology of the origin of isotope effect. Phys.Sci. Int. J 18: 1-11.
14. Ferrari AC, Bonaserco F, Fal'ko V, Konstantin S Novoselov, Stephan Roche, et al. (2015) Science and technology road map for graphene, related two - dimensional crystals and hybrid systems. Nanoscale 7: 4598-4810.
15. Bilz H, Kress W (1979) Phonon Dispersion Relation in Insulators. (Springer - Verlag, Berlin - Heidelberg).
16. Agekyan VF, Asnin VM, Kryukov AM (1989) Isotope effect in germanium. Fiz. Tverd. Tela (St. Petersburg) 31: 101-104.
17. Chrenko RM (1988) 13C - doped diamond: Raman spectra. J. Appl. Phys 63: 5873-5875.
18. Hanzawa H, Umemura N, Nisida Y (1996) Direct effects of nitrogen impurities, and 13C isotope composition on the Raman spectrum 1b diamond. Phys. Rev. B 54: 3793-3799.
19. Ramdas AK, Rodriguez S (1999) Lattice vibrations and electronic excitation in isotopically controlled diamonds. phys. stat. sol. (b) 215: 71-80.
20. Plekhanov VG (2004) Giant Isotope Effect in Solids. Stefan University Press, LA Jola, CA.
21. Plekhanov VG (2018) Introduction to Isotopic Materials Science (Springer, Heidelberg).
22. Plekhanov VG (2012) Isotopic effect renormalization of the energy of electrons by strong nuclear interaction. Deposit. in VINITI (Moscow) 13: N202 B2012.
23. Plekhanov VG (2021) Hadron - Lepton Interaction. LAMBERT Academic Publishing, Germany.
24. Boos EE (2022) The SMEET formalism: the basis for find in deviations from the Standard Model. Phys. - Uspekhi 65: 653-678.
25. Ioffe BL (2001) Chiral effective theory of strong interaction. Phys. - Uspekhi 44: 1211-1228.
26. Ioffe BL (2006) The origin of mass and experiments on high - energy particle accelerators. Phys. - Uspekhi 176: 1103-1104.
27. Karshenboim SG (2010) Constraints on a long - range spin - independent interaction from precision atomic physics. Phys. Rev. D 82: 073003-073005.
28. Delaunay C, Soreq Y (2017) Probing new physics with isotope shift spectroscopy. Phys. Rev. D 96: 115002-115006.
29. Delaunay C, Ozer R, Perez G (2017) Probing atomic Higgs - like forces at the precision frontier. Phys. Rev. D 96: 093001-093007.
30. Berengut JC, Budker D, Delaunay C (2018) Probing new long - range interactions by isotope shift spectroscopy. Phys. Rev. Lett 130: 091801-091807.
31. Frugiuele C, Fuchs E, Perez G (2017) Constraining new physics models with isotope shift spectroscopy. Phys. Rev. D 96: 0150117-015111.
32. Flambaum VV, Geddes AJ, Viatkina AV (2018) Isotope shift, non - linearity of King plots and the search for new particles. ArXiv/Physics. atom - ph/1709.00600.
33. Dzuba VA, Flambaum VV (2025) Using the Th III ion for a nuclear clock and searches for new physics. ArXiv/ Physics. atom - ph/ 2412.1308.
34. Sobel'man II (1964) Introduction to the Atomic Spectra. Science, Moscow.
35. Pekar SI (1964) Investigation into the electron Theory of Crystals. Academy- Verlag, Berlin.
36. Born M, Huang K (1954) Dynamical theory of Crystal Lattice. Clarendon Press, Oxford.
37. Plekhanov VG (2019) Measurements of the wide value range strong nuclear interaction coupling constant. SSRG Intern. J. Apll. Phys 6: 32-37.

38. Plekhanov VG (2005) Elementary excitations in isotope - mixed crystals. Phys. Reports 410: 1-235.
39. Breit G (1958) Theory of isotope shift. Rev. Mod. Phys 30: 507-516.
40. Alexandrov YuF (1982) Fundamental Properties of the Neutrons. Energoizdat, Moscow.
41. Yukawa Y (1935) On the interaction of elementary particles. Proceed. Phys. Math. Soc. (Japan) 17: 48-37.
42. Wallace PR (1947) The band theory of graphite. Phys. Rev 71: 622-629.
43. Slonczewski JC (1958) Band structure of graphite. ibid 109: 272-279.
44. Charlier JC, Blasé X, Roche S (2007) Electronic and transport properties of nanotubes. Rev. Mod. Phys 79: 677-732.
45. Huang M, Yan H, Chen C (2009) Raman spectroscopy of graphene under uniaxial stress: phonon softening and determination of crystallographic orientation. Proceed. Natl. Acad. Sci. USA 106: 7304-7315.
46. Ni ZhH, Yu T, Lu YH (2009) Uniaxial strain on graphene: Raman spectroscopy study and band - gap opening. ACS Nano 3: 483-492.
47. Mohiuddin TM, Lombarto A, Nair RR (2009) Uniaxial strain in graphene by Raman spectroscopy: G peak splitting, Grűneisen parameter and sample orientation. Phys. Rev. B 79: 205433-205438.
48. Han MY, Ozyilmaz B, Zhang Y (2007) Energy band - gap engineering of graphene nanoribbons. Phys. Rev. Lett 98: 206805-206814.
49. Ponomarenko LA, Schedin F, Katsnelson M (2008) Chaotic Diracbilliard in graphene quantum dots. Science 320: 356-358.
50. Savchenko A (2009) Transforming graphene. Science 323: 589-590.
51. Elias DC, Nair RR, Mohiuddin TMG (2009) Control of graphene properties by reversible hydrohenation: Evidence for graphene. ibid 323: 610-613.
52. Farjam M, Rafii – Tabar H (2009) Comment on Band structure engineering of graphene by strain: First - Principles calculations. Phys. Rev. B 80: 167401-167413.
53. Chen Sh, Wu Q, Mishra C, Hengji Zhang, Junyong Kang, et al. (2012) Thermal properties of isotopically engineering graphene. Natur. Mater 11: 203-207.
54. Kun C, Yu LQ, Bo T (2014) Isotope effect of the phonons mean free path in graphene by micro - Raman measurement. Science China, Phys., Mech. and Astro 57: 1817-1821.
55. Herrero CP, Ramirez R (2020) Isotopic effect in structural properties of graphene. Eur. Phys. J. B 93: 146-158.
56. Sofo JO, Chauhari AS, Barber A (2007) Graphane: A two - dimensional hydrocarbon. Phys. Rev. B 75: 154401-153414.
57. Nair RR, Ren WC, Riaz J (2010) Fluorographene two – dimensional counter part of Teflon. Small 6: 2877-2884.
58. Kenichi Sasaki (2018) Massive Dirac fermions signal in Raman spectrum of graphene. Phys. Rev. B 97: 115413-115416.
59. Roberts CD (2015) Hadron physics and QCD: Just the basic facts. ArXiv:nucl. th/1501.06581.
60. Roberts CD (2020) Empirical consequences of emergent mass. Symmetry 12: 1468-1506.